UC Davis
UC Davis Previously Published Works

Title

Collective cell migration has distinct directionality and speed dynamics

Permalink

https://escholarship.org/uc/item/14x0b739

Journal

Cellular and Molecular Life Sciences, 74(20)

ISSN

1420-682X

Authors

Zhang, Yan

Xu, Guoqing

Lee, Rachel M

et al.

Publication Date

2017-10-01

DOI

10.1007/s00018-017-2553-6

Peer reviewed

Cellular and Molecular Life Sciences

ORIGINAL ARTICLE

CrossMark

Collective cell migration has distinct directionality and speed dynamics

Yan Zhang[1,2,3] · Guoqing Xu[4,5] · Rachel M. Lee[6] · Zijie Zhu[3] · Jiandong Wu[4] ·
Simon Liao[5] · Gong Zhang[7,8] · Yaohui Sun[1] · Alex Mogilner[9] · Wolfgang Losert[6] ·
Tingrui Pan[3] · Francis Lin[4] · Zhengping Xu[2] · Min Zhao[1,10]

Abstract When a constraint is removed, confluent cells migrate directionally into the available space. How the migration directionality and speed increase are initiated at the leading edge and propagate into neighboring cells are not well understood. Using a quantitative visualization technique—Particle Image Velocimetry (PIV)—we revealed that migration directionality and speed had strikingly different dynamics. Migration directionality increases as a wave propagating from the leading edge into the cell sheet, while the increase in cell migration speed is maintained only at the leading edge. The overall directionality steadily increases with time as cells migrate into the cell-free space, but migration speed remains largely the same. A particle-based compass (PBC) model suggests cellular interplay (which depends on cell–cell distance) and migration speed are sufficient to capture the dynamics of migration directionality revealed experimentally. Extracellular Ca^{2+} regulated both migration speed and directionality, but in a significantly different way, suggested by the correlation between directionality and speed only in some dynamic ranges. Our experimental and modeling results reveal distinct directionality and speed dynamics in collective migration, and these factors can be regulated by extracellular Ca^{2+} through cellular interplay. Quantitative visualization using PIV and our PBC model thus provide a powerful approach to dissect the mechanisms of collective cell migration.

Keywords Wound healing · Cell contractility · PDMS · Corneal epithelial cell · Cell communication · Blebbistatin

Abbreviations
PBC   Particle-based compass
PDMS   Polydimethylsiloxane
PIV   Particle image velocimetry

✉ Francis Lin
  flin@physics.umanitoba.ca

✉ Zhengping Xu
  zpxu@zju.edu.cn

✉ Min Zhao
  minzhao@ucdavis.edu

1   Department of Dermatology, University of California, Davis, CA 95616, USA

2   Institute of Environmental Medicine, Zhejiang University School of Medicine, 866 Yuhangtang Rd., Hangzhou 310058, China

3   Micro-Nano Innovations (MiNI) Laboratory, Department of Biomedical Engineering, University of California, Davis, CA 95616, USA

4   Department of Physics and Astronomy, University of Manitoba, Winnipeg, MB R3T 2N2, Canada

5   Department of Applied Computer Science, University of Winnipeg, Winnipeg, MB R3B 2E9, Canada

6   Department of Physics, University of Maryland, College Park, MD 20742, USA

7   Seven Oaks Hospital Wellness Institute, 1075 Leila Ave, Winnipeg, MB R2P 2W7, Canada

8   The First Affiliated Hospital of Henan University of Science and Technology, 24 Jinghua Rd, Luoyang 471003, China

9   Courant Institute and Department of Biology, New York University, 251 Mercer Street, New York, NY 10012, USA

10 Department of Ophthalmology and Vision Science, University of California, Davis, CA 95616, USA

Introduction

Directionality and speed are two critical parameters in cell migration. When cells migrate in isolation, speed and directionality are regulated by different mechanisms, which orchestrate distinct cellular migratory behavior in different types of cells [1–7]. For example, *Dictyostelium* cells and neutrophil-like cells immobilized with latrunculin, which sequesters actin monomers and thus leads to degradation of actin filaments and decreases cell speed, are still capable of sensing chemoattractant gradients and establishing directionality [1].

Cells migrate collectively in wound healing, embryo development, tissue regeneration, and cancer metastasis [8]. How directionality and speed are regulated in collective migration is not well understood. Collective cell migration is not just simply the sum of the migration of a large group of individual cells. Collectively, cells migrate more efficiently in response to many directional cues than cells which migrate separately [9–12]. A cellular interplay has been proposed as the mechanism that underlies the increased efficiency in collective migration [8, 13]. This interplay may include biochemical and mechanical interactions such as propelling forces transmitted through cell–cell contacts [14, 15], contact-dependent cell polarity [11], adherens junction treadmilling [16], contact inhibition of locomotion [12, 17], and secreted molecules [18].

Monolayer wound healing assays are widely used in the study of collective cell migration. The barrier model allows cells to become confluent next to a barrier [19]. Cells migrate directionally toward the cell-free surface after removing the barrier. Advantages of the barrier-removal assay include that the cells at the edge are not damaged as in the scratch assay, and that the cells move over a surface on which the substratum is not affected by the scratching process [14, 15, 19–24]. Direction cues in this system may include space availability, population pressure, contact inhibition of locomotion, and activation of EGFR [25, 26].

Particle image velocimetry (PIV) is a cross-correlation technique initially developed in the field of hydrodynamics, which has been proven to be a useful tool for characterizing local displacements and has been used to study velocity dynamics in collective cell migration [27–30]. To investigate the transmission of directional movement signals from the free edge into a large sheet of corneal epithelial cells, we used PIV to quantitatively analyze and visualize collective cell migration with the detailed distinction between directionality and speed. Our results reveal remarkable distinctions between directionality and speed dynamics during collective migration of an epithelial cell confluent culture.

To investigate how cellular interplay may regulate migration directionality and speed in collective migration,

we developed a particle-based compass (PBC) mathematical model. The key parameter for cellular interplay in this PBC model is the particle–particle distance (i.e., cell–cell distance). Following suggestions from the model, we experimentally tested the effects of extracellular Ca^{2+} on collective migration. We chose Ca^{2+} because early in the wound healing process, the concentration of Ca^{2+} in the wound fluid changes [31] and Ca^{2+} plays a significant role in membrane protrusion and cell–cell adhesion [32–34], which presumably underlie cellular interplay. Indeed, we find that Ca^{2+} plays different roles in regulating directionality and speed changes in collective migration of corneal epithelial cells.

Materials and methods

Reagents and cell line

Telomerase-immortalized human corneal epithelial cells (hTCEpi) were cultured at 37 °C, 5% CO_2 in EpiLife medium containing 60 μM Ca^{2+} (Life Technologies, USA) supplemented with an EpiLife defined growth supplement (EDGS, Life Technologies, Grand Island, USA) and 1% (v/v) penicillin/streptomycin (Life Technologies). For Ca^{2+} intervention groups, 1 h before imaging, cell culture medium was switched to medium with high or low Ca^{2+}. For low-Ca^{2+} experiments, 1 mM EGTA or 2 mM EGTA was added. For high-Ca^{2+} experiments, the medium was supplemented with an additional 60 μM or 120 μM Ca^{2+}. For cell contractility intervention groups, 50 μM blebbistatin (a selective membrane-permeant inhibitor for non-muscle myosin II ATPase) was added 2 h before imaging. For the relative control group, DMSO (dimethyl sulfoxide) (1 μl/ml) was added. EGTA, $CaCl_2$, DMSO, and blebbistatin were purchased from Sigma-Aldrich (St. Louis, MO, USA).

Wound model

Before seeding the cells, PDMS strips were deposited on the surface of a six-well cell culture dish pre-coated with FNC (an aqueous solution of fibronectin and other cell adhesion proteins). 16–18 h after seeding, a confluent monolayer of cells was formed. Before image recording, the PDMS barrier was lifted with sterile tweezers to create a space next to the monolayer, and a clear and straight edge was left behind.

Time-lapse microscopy

Migration of cells from the edge of the wound was imaged by phase-contrast microscopy using an inverted microscope (Carl Zeiss, Oberkochen, Germany) equipped with a motorized stage, a specialized time-lapse imaging software

(Metamorph NX; Molecular Device, Sunnyvale, USA) and a Carl Zeiss incubation system. A regular 10× objective lens was used for microscopy. Imaging began 10 min after wounding. The interval between image acquisitions was 5 min, and a typical experiment lasted for 6 h. To capture cell behavior over scales up to 0.5 mm behind the free edge, two images that covered the area of cell culture were acquired at each time point and were stitched together using Image J software from the National Institutes of Health (http://rsbweb.nih.gov/ij/).

Individual cell tracking

ImageJ software (MTrackJ) was used to quantify migration directionality and speed. Monolayer boundaries were computed by tracking ten points on the edge of the wound and computing an average to track the edge. For analysis of region dependence in cell migration during wound healing, we divided the first 15 rows of cells from the free edge into rows of 5 cells and defined them as the leading region, transition region, and trailing region, as illustrated in Supplementary Fig. S2a. The position of a cell was defined by its nuclear centroid. For each region, more than 70 cells in the monolayer were tracked at 10-min intervals. Directionality was defined as the cosine of the angle between cell trajectory and a line perpendicular to the free edge. A cell migrating directly toward the free surface (i.e., perpendicular to the free edge) would have a cosine equal to 1. Cells migrating directionless and randomly would have an average cosine equal to ~ 0. Cell migration speed is the accumulated migrated distance divided by time.

To analyze changes in cell density in collective cell migration, we quantified cell numbers in six regions of 160 μm width each, with the initial edge of cell sheets in the middle (Fig. S8a). Then we counted the cell numbers at 0, 3, and 6 h. Cell density was computed by dividing the cell number in each region by the area.

PIV migration analysis

Cell migration in the time-lapse images was quantified by PIV analysis using MATLAB (MathWorks) with a custom MATLAB code based on MatPIV1.6.1, a freeware distributed under the terms of the GNU general public license. The MATLAB code has been previously described in detail [35]. Kymographs were used to quantify and visualize spatiotemporal dynamics of horizontal velocity, directionality, and speed from the PIV measurements. For each data matrix from the PIV analysis, we computed the average value for each column parallel to the free edge and then derived a one-dimensional segment for each time point (Supplementary Fig. S4b). We defined the front of the directionality wave in the kymograph as the first grid of

at least seven consecutive grids that reached a directionality threshold of $\cos(\theta) \geq 0.2588$. Then we plotted the front of the directionality wave averaged over a defined time interval against each time point to obtain the best linear fit using the fitting equation $y = ax + b$, where x is the wave front position, y is the time, a is the slope of the linear fit, and b is the intercept of the linear fit. The propagation rate of the directionality wave was calculated as $R = 1/a$. (Supplementary Fig. S7) (please see the Supplementary Material for details).

PBC model

We developed a physical model based on wound healing assay experiments. All the length parameters were scaled such that 0.1 in model length units equaled 20 μm in real space (equivalent to the diameter of a single cell). The speed for the control group was set as 0.015 model length units (3 μm in real space) per simulation time step (4.8 min in real time), which is equivalent to the average speed of 37.3 μm/h measured in control group experiments. The space surrounding the center of a specific cell was divided into eight equal sectors (Fig. 2b, c). In our model, all cells were treated as particles with a diameter of 0.1. We assume that if the distance d between a specific cell and its nearest neighboring cell in a particular angular sector is less than the repulsive threshold distance D_0, the cell will have a repulsive interaction with the neighboring cell. The magnitude of this repulsive interaction is inversely proportional to d. If d is greater than the free edge threshold distance D_{max}, this specific cell is considered a free edge cell and will gain a contribution to its motion direction toward the free space. If d is between D_0 and D_{max}, a biased directionality of the specific cell toward the nearest neighboring cell is modeled. The magnitude of this biased directionality is directly proportional to d (Fig. 2d). This mechanism is applied to compute the cellular interplay in each of the eight angular sectors. By summing up the eight cell–cell interactions, the total cellular interplay vector for a specific cell can be obtained and the phase of this vector will be used to determine the cell migration angle. This algorithm is used to simulate collective cell migration in the experimental wound healing assay. In the control group simulations, D_0 is set at 0.12 (24 μm in real space) and D_{max} is set at 0.30 (60 μm in real space) to best match the experimental data. More details of the model construction and numerical simulations are provided in the Supplementary Material.

Statistics

Data analyses, graphs, and statistical calculations were performed using Excel (Microsoft) and MATLAB

(MathWorks). Data are presented as mean ± standard error of the mean (SEM) or mean ± standard deviation (SD). Differences between conditions were compared using Student's t test. The difference was considered statistically significant if $p < 0.05$.

Results

Outward collective migration was initiated from the free edge

To induce directional collective migration, we cultured human corneal epithelial cells against a polydimethylsiloxane (PDMS) barrier to confluence at ~18 h after seeding the cells. Upon removal of the barrier, cells migrated into the cell-free areas as previously reported with increases in the number of cells in the imaging field, decreases in cell-free area, and advancement of the leading edge cells into the cell-free area (Supplementary Fig. S1, Supplementary Video S1) [36]. Because of the short time period of imaging (3–6 h), increased cell numbers in the cell-free area were mainly due to cell migration and not cell proliferation. Examination of time-lapse videos showed that less than 2% of cells divided during this period.

Directionality waves propagated into the cell sheet

To visualize changes in directionality and speed of cell migration following free edge generation, we took advantage of PIV, which provides quantitative visualization of directionality and speed of the mass movement of whole cell groups. Remarkably, the directionality of cell movement into the cell-free area (X-directionality) first increased at the leading edge and then propagated into neighboring confluent cells (Fig. 1a; Supplementary Video S2), while changes in the speed of cell movement (i.e., cell migration speed) did not show propagation from the free edge into the following cells (Fig. 1b; Supplementary Video S2).

Kymographs of directionality and speed of migration confirmed the contrast between these two migration parameters. Increases in directionality at the free edge propagated into the cell sheet over time as a wave (blue arrow in Fig. 1c). Changes in cell migration speed, however, did not show a similar propagation (Fig. 1d). The fraction of cell motion directed to the free edge within a bias angle less than 60° or 45° increased over time (Fig. 1e), while the speed remained stable (Fig. 1f). The

directionality wave propagated into the cell sheet with a speed significantly higher than the speed at which the free edge advanced into the cell-free area (49.74 ± 33 vs. 34.66 ± 6.55 μm/h, $p < 0.05$).
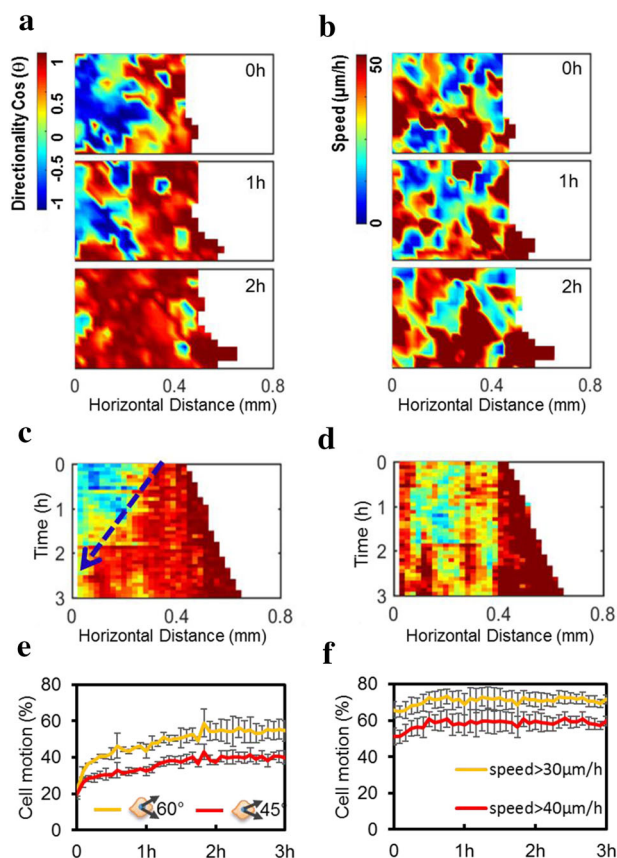

Fig. 1 Free edge induced a wave-like propagation of directionality but not the speed in confluent epithelial cells. **a** Heat maps of cell migration directionality at different time points show the increase in directionality as a wave propagating from the leading cells into the following cells after removal of the PDMS barrier. "Hot" colors like *red* show migration to the right, into the free space. "Cold" colors like *blue* show migration to the *left*, away from the free space. **b** Heat maps of cell migration speed, however, lack a similar wave propagation from the leading cells into the following cells. **c** Kymograph showing an increase in directionality propagating from the leading edge into the cell sheet along time (*blue arrow*); by 3 h, all the cells migrated directionally to the right (coded *red*). **d** Kymograph coding migration speed shows that speed increased at the leading edge, but did not propagate into the cell sheet. **e, f** After PDMS barrier removal, cells showed increased directionality: the proportion of cell motion directed to the free edge within a bias angle less than 60° or 45° increased over time (**e**), while the fraction of cells with a speed over 30 or 40 μm/h remained stable (**f**). Directionality and speed of cell migration were calculated using PIV (see "Materials and methods"). *Color* indicates the value of cosine theta (directionality) from −1 to 1 (**a**) or the cell speed from 0 to 50 μm/h (**b**). Data are presented as mean ± SD from three independent experiments

Tracking migration of individual cells validated PIV results

We then manually tracked cells to validate the results with those obtained using PIV analysis (Supplementary Fig. S2). We divided the first 15 rows of cells from the free edge into three regions which are 0–160, 160–320, and 320–480 µm from the free edge (Supplementary Fig. S2a). Migration trajectories of individual cells in each group were plotted with the initial position at the origin (Supplementary Fig. S2b–d). Cell migration showed gradually increased directionality starting from the leading edge: cells in the 0–160 µm region responded first with steady displacement into the cell-free area while cells in the 160–320 µm region (about five cell rows from the free edge) took 1–2 h to show directional displacement. Cells in the 320–480-µm region took even longer (2–3 h) to show directional cell migration (Supplementary Fig. S2b–e).
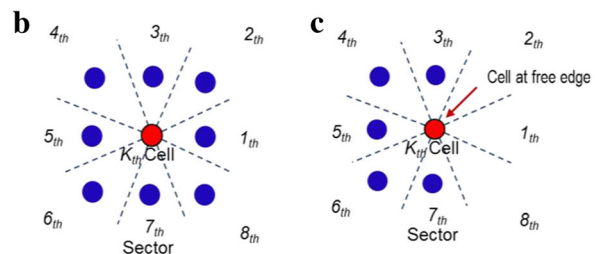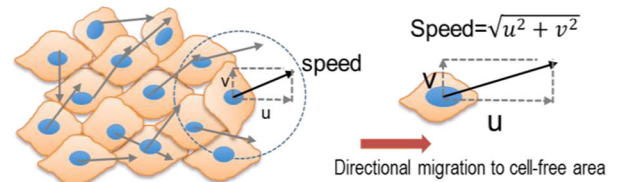
From the trajectory data, we further analyzed migration directionality and speed in each region. The directionality of the 0–160-, 160–320-, and 320–480-µm regions are significantly different in the first hour after barrier removal. Cells in the 0–160-µm region have significantly higher directionality into the cell-free area (perpendicular to the free edge) compared to cells in the other two regions. This difference gradually reduced as the cells in the 160–320- and 320–480-µm regions began to follow the leading edge (Supplementary Fig. S3a, b). The mean speed of the cells in all three regions remained the same (Supplementary Fig. S3c, d). Together with the speed and directionality measurements, these data indicated that directional guidance cues from the free edge extended gradually into the cell sheet in a spatial–temporal-dependent manner, but that the speed remained relatively stable. Manual tracking analysis confirmed the results from PIV analysis. A similar propagation pattern in the directional velocity was evident when the velocity of the movement into the cell-free area was visualized over time (Supplemental Fig. S4a, c), which was similar to previous reports of the leading edge movement in studies without detailed and separate analysis of directionality and speed.

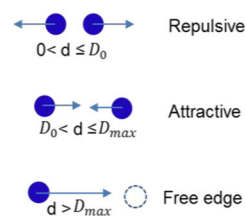## A PBC model reproduced the directionality propagation

To study how the migration directionality and speed are differentially regulated in collective cell migration, we developed a two-dimensional PBC model (please see Supplementary Material for details). Briefly, cells in a group tend to migrate into cell-free space (Fig. 2a). As cells at the free edge migrate, they move away from the cells behind, and experience reduced cell–cell contact inhibition (modeled as a repulsive interaction), as well as

biased migration of the cells toward the free space (modeled as an attractive interaction). Cells farther behind are then biased to migrate toward the cell-free area. Thus, in this model, we simplified cellular interplay to one factor, i.e., the particle–particle distance, which is mathematically defined as the distance between a specific cell and its immediately adjacent cells in each of the eight equally spaced angular sectors in a 2D plane (centered at the location of the specific cell) (Fig. 2b, c). Varying the threshold cell–cell distance parameters, i.e., D_0 for the transition from repulsive to attractive interaction and D_{max} for the transition from the distance-dependent attractive
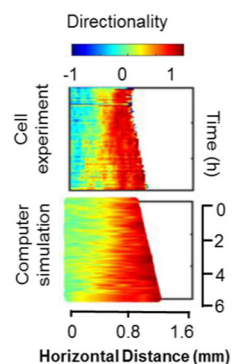

Fig. 2 PBC model to simulate collective migration. **a** Schematic of the model, which sets the speed of individual cells as particles and adjusts directionality depending on interactions with neighboring cells. **b–d** A particle representing a cell (*red dot*) at the free edge has three vacant neighbor sectors out of eight, which biases the direction of migration with the principles in **d**. The total cellular interplay for the kth cell is the sum of the eight interactions. Particle–particle distance d determines the cellular interactions, where D_0 and D_{max} denote the threshold of repulsive and the threshold of the free surface effect. When $0 < d \leq D_0$, the particle is repulsed; when $D_0 < d \leq D_{max}$, the particle is attracted; and when $d > D_{max}$ the cell feels a contribution from the free edge. **e** A kymograph from the model shows a pattern of directionality propagation similar to the experimental results. Computer simulation with repulsive threshold $D_0 = 0.12$ (24 µm) and average speed $= 37.3$ µm/h

interaction to the free edge biased migration, mediates the dynamics of cell migration directionality (Fig. 2d). We set cell speed to be a constant plus noise in the model, because our experiments showed stable migration speeds (Fig. 1f).

Computer simulations based on this PBC model showed similar pattern of directional collective migration as cell culture experiments. Cells close to the free edge migrate directionally first and the cells behind follow in a time-dependent manner (Supplementary Video S3). Kymographs of directionality from the simulation show similar patterns to that from the experiment (Fig. 2e). We used D_0 and migration speed as two major model parameters. In initial simulations, we set the migration speed constant according to cell culture experiments (Fig. 1f) and varied the repulsive interaction threshold D_0. D_0 is crucial to determine the propagation rate of the directionality wave (Fig. 3a, c). Holding D_0 constant and varying migration speed also affected directionality wave propagation (Fig. 3b, d). However, it is worth noting that the directionality propagation rate is less sensitive to the speed when the speed is over a certain threshold value at a defined D_0 (Fig. 3d).

Different roles of Ca^{2+} in propagation of speed and directionality waves

To examine mechanisms of directionality wave propagation, we manipulated extracellular Ca^{2+}. EGTA, a Ca^{2+} chelator, significantly slowed down cell migration (Fig. 4a, b; Supplementary Fig. S5a, b, Video S4, 5). EGTA treatment at both 1 mM and 2 mM reduced migration speed to a similar level (Fig. 4a, b). However, the effects of 1 and 2 mM EGTA on directionality were different in that 2 mM EGTA almost abolished migration directionality, while cells in 1 mM EGTA maintained obvious directionality (Fig. 4a).

Addition of higher Ca^{2+} to 60 or 120 μM did not increase the average speed of cell migration (Fig. 4a, b; Supplementary Fig. S6a, b, Video S4, 6), however, the rate of directionality wave propagation was significantly elevated (Fig. 4a, c). The fraction of cell motion in the sheet with a bias angle less than 60° in the control, EGTA 2 mM, Ca^{2+} 120 μM groups confirmed these differences in directionality propagation (Supplementary Fig. S6c). The time course of the fraction of cell motion in the sheet with migration speed 40 μm/h above for control, EGTA 2 mM, and high-Ca^{2+} groups also confirmed the effect on migration speed (Fig. 4b). These same experiments also showed that the directionality wave propagated faster across the monolayer when Ca^{2+} was increased (Fig. 4c).

We then investigated how Ca^{2+} regulates propagation of the directionality wave—whether it is through its effect on migration speed, on the interaction threshold (D_0), or on both. In the PBC model, two major parameters that affected directionality wave propagation were speed and the
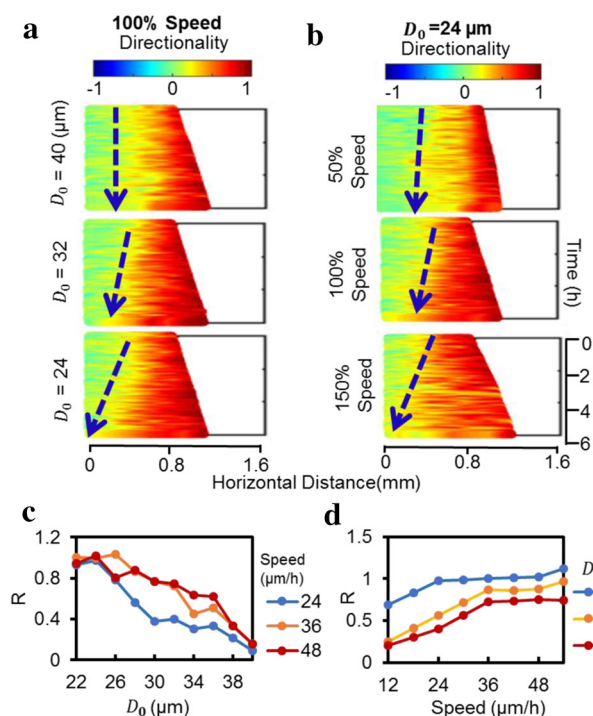

Fig. 3 Computer simulations suggested D_0 and speed as two major parameters that affect directionality wave propagation. **a** Effect of repulsive threshold D_0 (24, 36 or 40 μm) on directionality wave propagation. Speed is set at 37.3 μm/h. D_0 is the threshold of repulsive interactions. The value ranges from 24 to 40 μm. Decreasing D_0 accelerated wave propagation. **b** Effect of speed (50, 100, 150% of the control speed of 37.3 μm/h) on directionality wave propagation. Repulsive threshold $D_0 = 24$ μm. The value ranges from 0 to 150% (12–55 μm/h). Increasing speed accelerates wave propagation. **c**, **d** The rate of directionality wave propagation depends on D_0 and particle speed. R is the normalized rate of directionality wave propagation. R was set as 1 when $D_0 = 24$ μm and speed = 37.3 μm/h. D_0 negatively correlated with the rate, whereas the rate was positively correlated with speed

repulsive action threshold, D_0. In high-Ca^{2+} experiments, there was no apparent change in cell speed (Fig. 5a), thus D_0 must be decreased to cause an increase in the propagation rate of directionality wave (Fig. 5c). EGTA treatment decreased the speed of cell migration, which reduced the directionality wave propagation. The average speed of cell migration was significantly reduced after EGTA treatment: 27.47 and 32.92% of that in the control value in 1 and 2 mM EGTA, respectively (Fig. 5a). We simulated cells using 30% of the control group cell speed but with the same D_0 as in the control group. The simulation results suggested that simply reducing the cell speed to 30% was insufficient to inhibit the directionality wave propagation (Fig. 5b). An increase in D_0 along with reduced cell speed produced a directionality wave pattern consistent with the experimental results (Fig. 5b), suggesting that EGTA treatment affected both cell speed and cellular interplay, which in combination inhibited
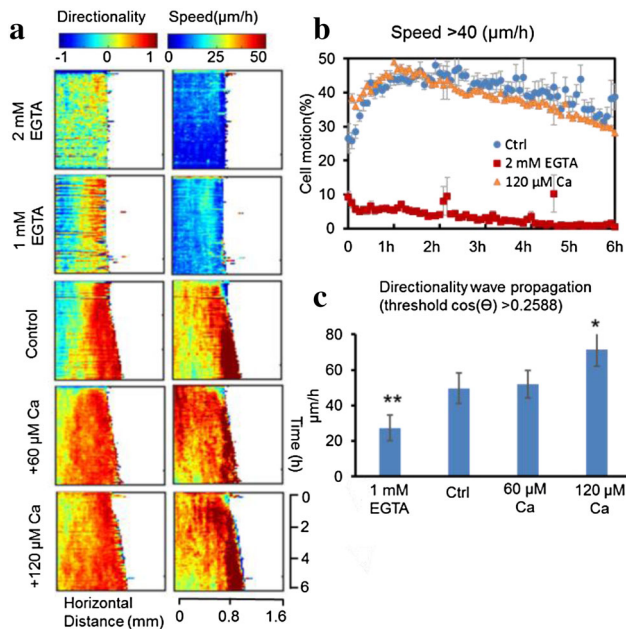
Fig. 4 Calcium regulates the propagation of directionality waves. **a** Extracellular Ca^{2+} significantly affects directionality and speed for cell migration. Kymographs show that Ca^{2+} had different effects on directionality wave propagation and speed. **b** High Ca^{2+} did not affect migration speed. The graph shows the time course of the proportion of cells in the sheet reaching a speed >40 μm/h for control, EGTA 2 mM, calcium 120 μM groups. **c** High extracellular Ca^{2+} increased, while depletion of Ca^{2+} decreased, the rate of directionality wave propagation. $*p < 0.05$, $**p < 0.01$ when compared with the control value using a Student's t test. Data of the proportion of cells reaching a certain threshold over time are mean ± SEM from three independent experiments. Data on wave propagation rates are mean ± SEM from four independent wounds

directionality wave propagation. In high-Ca^{2+} simulations, a change in D_0 alone was able to recapitulate experimental observations of directionality wave propagation (Fig. 5c).

Directionality wave propagation is independent of cell contractility

To investigate the role of myosin in directionality wave propagation, we used blebbistatin, an inhibitor for non-muscle myosin II ATPase. After peeling off the PDMS barrier, both the blebbistatin-treated group and the control group migrated directionally toward the cell-free area. Blebbistatin-treated cells became elongated with an extend cell body dragging behind as previously reported [37–39] (Supplementary Video S7). No significant difference was found in the distance between cells (cell density) along the x-axis (Fig. S8b), advancement of the leading edge into the cell-free area (Fig. S8c), directionality wave propagation (Fig. S8d), time evolution of directionality (Fig. S8e), and cell migration speed (Fig. S8f) between the blebbistatin-treated group and the control group.
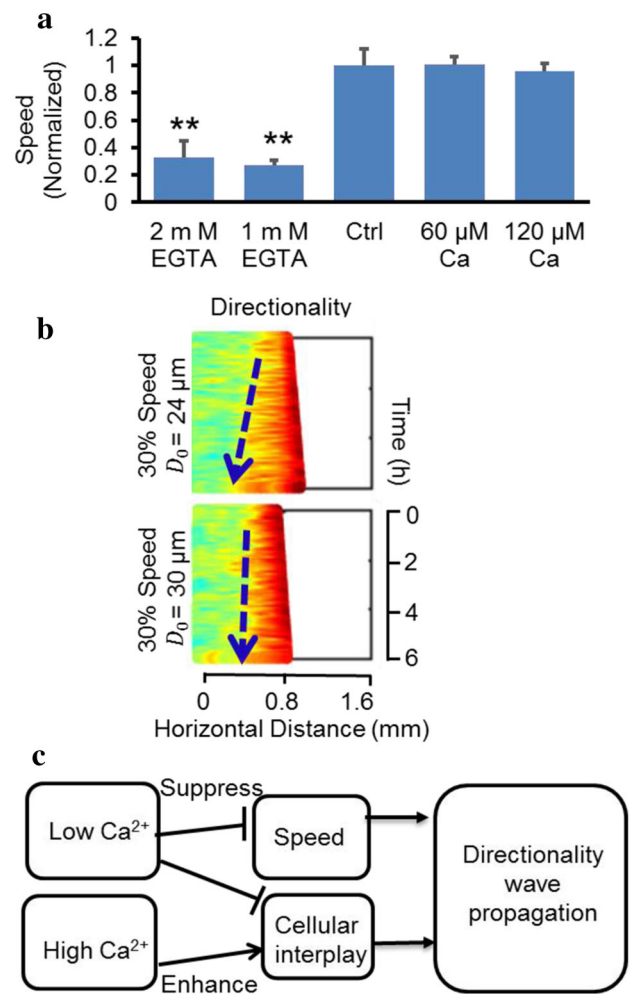

Fig. 5 Hypothetical effects of Ca^{2+} on the propagation of directionality wave through speed and cellular interplay. **a** Depletion of Ca^{2+} reduced migration speed to 30% of the control. The average speed of the control group is normalized to 1, and average speed of EGTA groups is about 0.3. **b** Simulation results from the simulation model indicate that when cell speed is tuned down to 30% of the control value with other parameters unchanged, the directionality wave keeps propagating for a considerable distance. A combination adjustment of speed and D_0 reproduces a kymograph similar to the EGTA experimental data (Fig. 4a). **c** The schematic diagram shows how Ca^{2+} affects directionality waves through cell speed and cellular interplay. Low Ca^{2+} reduces speed and cellular interplay (increasing D_0), and thus decreases directionality wave propagation. High Ca^{2+} increases cellular interplay (decreasing D_0) and enhances directionality wave propagation with little effect on the speed. Data are shown as mean ± SEM from three independent experiments. $*p < 0.05$, $**p < 0.01$

Discussion

In this study, we used PIV-based techniques to reveal different dynamics in directionality and speed in collective cell migration. In confluent human corneal epithelial cells, a directionality wave was initiated at the leading edge when constraint was removed, and the directionality wave

propagated backward into the cell sheet while migration speed remained unchanged. PBC modeling suggested two parameters—cell–cell distance and migration speed—could control the rate of the directionality wave propagation. Experimental tests of this prediction using Ca^{2+} showed that changes in "cellular interplay" and cell migration speed can regulate directionality wave propagation.

PIV analysis of cell movement relies on basic pattern matching instead of tracking individual cells to quantify cell movement. No labeling is required and many types of microscope images meet the requirements for the analysis. PIV provides significantly detailed parameters for collective cell migration, including directionality and speed in all directions over the whole cell area. These parameters can be analyzed and, importantly, visualized with high spatial and temporal resolution over a large size of field [40]. Traditional manual tracking of individual cells confirmed the reliability of PIV analysis. Thus, PIV has been widely used in quantify and visualize collective cell migration [14, 27–30]. Visualization of cell sheet movement using PIV revealed striking propagation of a directionality wave from the leading edge cells to the inside of the cell sheet (Fig. 1a, c), whereas the increase in migration speed was localized to cells at the leading edge (Fig. 1b, d). In other words, the directionality signal can be transmitted independently of changes in cell migration speed. In both chemotaxis and galvanotaxis of isolated cells, speed and directionality of migration have been suggested to have different control mechanisms [5–7]. Systematic screening of the signaling pathways involved in the collective migration of endothelial cells has revealed the molecular basis for independent functional modules, such as proliferation, cell migration speed, directed migration, and cell–cell coordination [41]. Quantitative visualization of directionality and speed in collective cell migration will facilitate understanding of these mechanisms. Some aspects have been reported before in different context [24, 39, 42]. For example, previous work found that directionality waves keep propagating for some time, even after the two advancing edges of cell groups meet, which suggests that the free edge is necessary for directional migration of the cells at edge, but not essential for propagation of the directionality wave [24].

Multiple models of collective cell migration have been reported to simulate force transmission between cells [14], the generation of finger cells [43, 44], the advancement of free edges [45] and other features of collective migration, but little has been done on cell migration velocity evolution in wound healing. Similar particle-based modeling has been used to simulate collective migration [43, 46]. Sepulveda et al. have elegantly demonstrated cell motion at early stages after barrier removal, as well as the formation of leader cells and fingers at the free edge [43]. Long-term effects of barrier removal and the cell migration dynamics behind free edge, however, have not been investigated. On the other hand, compass modeling has been used for simulating cell polarity/asymmetry and planar cell polarity signaling in isolated individual cells [47–50]. Our PBC model for collective cell migration integrates directional cues from neighboring angular sectors. This model simplifies the complex cellular interactions and provides an approximated approach to capture directionality wave propagation. It offers a quick in silico test for the key parameters that may affect collective cell migration (Figs. 2, 3).

For this particular corneal epithelial cell line, we observed that some cells at the edge migrated away from the group. We also noticed that neighboring cells did not attach by forming tight cell–cell junctions. Nonetheless, the robust transition of directionality persists both experimentally and in simulations, which suggests that cell–cell mechanical coupling is not essential for transmission of directional signals, although it has been suggested to be required for collective migration of MDCK cells [14].

Extracellular Ca^{2+} regulates many aspects of cell migration including polarity [34, 51–54], migration speed [34, 55–57], cell–cell adhesion (e.g., cadherin-based adhesions) [51, 58], and membrane protrusion. In collective cell migration, additional Ca^{2+} promoted directionality wave propagation. The propagation rate of directionality waves was significantly higher than that of the control group (Fig. 4a, c), whereas migration speed in high-Ca^{2+} conditions was the same as the control group, suggesting that high-Ca^{2+}-accelerated directionality wave propagation was independent of cell migration speed. Simulations indicated that the reduction in speed could not fully account for inhibition of the directionality wave propagation (Fig. 5b, c). This is supported by experiments which showed that only 120 μM Ca^{2+} significantly increased the directionality wave propagation, whereas cells in both 60 and 120 μM Ca^{2+} had the same speed (Fig. 5a). Low-Ca^{2+} levels affected cell migration speed (Fig. 4b) and also affected the collective directional response, presumably through cellular interplay. These results provide further evidence for the separation of directionality and speed in collective cell migration and suggest regulation by Ca^{2+}, which warrants further investigation to elucidate downstream mechanisms underlying different regulation of directionality and speed of collective migration by Ca^{2+}.

In summary, PIV analysis revealed that a free edge in corneal epithelial monolayer induced a directionality wave of cell migration propagating from the leading edge over several hundred microns into the following confluent cells, whereas the increase in cell migration speed was limited to the leading edge cells. The directionality wave was

differentially regulated by extracellular Ca^{2+}, presumably through cellular interplay and migration speed.

Compliance with ethical standards

Conflict of interest The authors declare no conflict of interest.

References

1. Devreotes P, Janetopoulos C (2003) Eukaryotic chemotaxis: distinctions between directional sensing and polarization. J Biol Chem 278(23):20445–20448. doi:10.1074/jbc.R300010200
2. Servant G, Weiner OD, Herzmark P, Balla T, Sedat JW, Bourne HR (2000) Polarization of chemoattractant receptor signaling during neutrophil chemotaxis. Science 287(5455):1037–1040
3. Parente CA, Blacklock BJ, Froehlich WM, Murphy DB, Devreotes PN (1998) G protein signaling events are activated at the leading edge of chemotactic cells. Cell 95(1):81–91. doi:10.1016/S0092-8674(00)81784-5
4. Ridley AJ, Schwartz MA, Burridge K, Firtel RA, Ginsberg MH, Borisy G, Parsons JT, Horwitz AR (2003) Cell migration: integrating signals from front to back. Science 302(5651):1704–1709. doi:10.1126/science.1092053
5. Bültmann BD, Gruler H (1983) Analysis of the directed and nondirected movement of human granulocytes: influence of temperature and ECHO 9 virus on N-formylmethionylleucylphenylalanine-induced chemokinesis and chemotaxis. J Cell Biol 96(6):1708–1716
6. Gruler H, Franke K (1990) Automatic control and directed cell movement. Novel approach for understanding chemotaxis, galvanotaxis, galvanotropism. J Biosci 45(11–12):1241–1249
7. Gruler H, Nuccitelli R (2000) The galvanotaxis response mechanism of keratinocytes can be modeled as a proportional controller. Cell Biochem Biophys 33(1):33–51. doi:10.1385/CBB:33:1:33
8. Friedl P, Gilmour D (2009) Collective cell migration in morphogenesis, regeneration and cancer. Nat Rev Mol Cell Biol 10(7):445–457
9. Li L, Hartley R, Reiss B, Sun Y, Pu J, Wu D, Lin F, Hoang T, Yamada S, Jiang J, Zhao M (2012) E-cadherin plays an essential role in collective directional migration of large epithelial sheets. Cell Mol Life Sci 69(16):2779–2789. doi:10.1007/s00018-012-0951-3
10. Zhao M, Agius-Fernandez A, Forrester JV, McCaig CD (1996) Directed migration of corneal epithelial sheets in physiological electric fields. Invest Ophthalmol Vis Sci 37(13):2548–2558
11. Theveneau E, Marchant L, Kuriyama S, Gull M, Moepps B, Parsons M, Mayor R (2010) Collective chemotaxis requires contact-dependent cell polarity. Dev Cell 19(1):39–53
12. Mayor R, Carmona-Fontaine C (2010) Keeping in touch with contact inhibition of locomotion. Trends Cell Biol 20(6):319–328. doi:10.1016/j.tcb.2010.03.005
13. Mayor R, Etienne-Manneville S (2016) The front and rear of collective cell migration. Nat Rev Mol Cell Biol 17(2):97–109. doi:10.1038/nrm.2015.14
14. Serra-Picamal X, Conte V, Vincent R, Anon E, Tambe DT, Bazellieres E, Butler JP, Fredberg JJ, Trepat X (2012) Mechanical waves during tissue expansion. Nat Phys 8(8):628–634
15. Das T, Safferling K, Rausch S, Grabe N, Boehm H, Spatz JP (2015) A molecular mechanotransduction pathway regulates collective migration of epithelial cells. Nat Cell Biol 17(3):276–287
16. Peglion F, Llense F, Etienne-Manneville S (2014) Adherens junction treadmilling during collective migration. Nat Cell Biol 16(7):639–651
17. Cheng G, Youssef BB, Markenscoff P, Zygourakis K (2006) Cell population dynamics modulate the rates of tissue growth processes. Biophys J 90(3):713–724
18. Weijer CJ (2004) Dictyostelium morphogenesis. Curr Opin Genet Dev 14(4):392–398
19. Das AM, Eggermont AM, ten Hagen TL (2015) A ring barrier-based migration assay to assess cell migration in vitro. Nat Protoc 10(6):904–915. doi:10.1038/nprot.2015.056
20. Etienne-Manneville S, Hall A (2001) Integrin-mediated activation of Cdc42 controls cell polarity in migrating astrocytes through PKCzeta. Cell 106(4):489–498
21. Etienne-Manneville S, Hall A (2003) Cdc42 regulates GSK-3beta and adenomatous polyposis coli to control cell polarity. Nature 421(6924):753–756. doi:10.1038/nature01423
22. Raftopoulou M, Etienne-Manneville S, Self A, Nicholls S, Hall A (2004) Regulation of cell migration by the C2 domain of the tumor suppressor PTEN. Science 303(5661):1179–1181. doi:10.1126/science.1092089
23. Klarlund JK (2012) Dual modes of motility at the leading edge of migrating epithelial cell sheets. Proc Natl Acad Sci USA 109(39):15799–15804. doi:10.1073/pnas.1210992109
24. Zaritsky A, Kaplan D, Hecht I, Natan S, Wolf L, Gov NS, Ben-Jacob E, Tsarfaty I (2014) Propagating waves of directionality and coordination orchestrate collective cell migration. PLoS Comput Biol 10(7):e1003747
25. Klarlund JK, Block ER (2011) Free edges in epithelia as cues for motility. Cell Adhes Migr 5(2):106–110
26. Block ER, Tolino MA, Lozano JS, Lathrop KL, Sullenberger RS, Mazie AR, Klarlund JK (2010) Free edges in epithelial cell sheets stimulate epidermal growth factor receptor signaling. Mol Biol Cell 21(13):2172–2181
27. Chepizhko O, Giampietro C, Mastrapasqua E, Nourazar M, Ascagni M, Sugni M, Fascio U, Leggio L, Malinverno C, Scita G, Santucci S, Alava MJ, Zapperi S, La Porta CA (2016) Bursts of activity in collective cell migration. Proc Natl Acad Sci USA 113(41):11408–11413. doi:10.1073/pnas.1600503113
28. Milde F, Franco D, Ferrari A, Kurtcuoglu V, Poulikakos D, Koumoutsakos P (2012) Cell image velocimetry (CIV): boosting the automated quantification of cell migration in wound healing assays. Integr Biol 4(11):1437–1447. doi:10.1039/c2ib20113e
29. Poujade M, Grasland-Mongrain E, Hertzog A, Jouanneau J, Chavrier P, Ladoux B, Buguin A, Silberzan P (2007) Collective migration of an epithelial monolayer in response to a model wound. Proc Natl Acad Sci USA 104(41):15988–15993. doi:10.1073/pnas.0705062104
30. Petitjean L, Reffay M, Graslandmongrain E, Poujade M, Ladoux B, Buguin A, Silberzan P (2010) Velocity fields in a collectively migrating epithelium. Biophys J 98(9):1790–1800
31. Grzesiak JJ, Pierschbacher MD (1995) Shifts in the concentrations of magnesium and calcium in early porcine and rat wound

fluids activate the cell migratory response. J Clin Investig 95(1):227

32. Lagunowich LA, Grunwald GB (1989) Expression of calcium-dependent cell adhesion during ocular development: a biochemical, histochemical and functional analysis. Dev Biol 135(1):158–171

33. Gipson IK (1992) Adhesive mechanisms of the corneal epithelium. Acta Ophthalmol 70(S202):13–17

34. Lawson MA, Maxfield FR (1995) Ca^{2+}-and calcineurin-dependent recycling of an integrin to the front of migrating neutrophils. Nature 377(6544):75–79

35. Lee RM, Kelley DH, Nordstrom KN, Ouellette NT, Losert W (2013) Quantifying stretching and rearrangement in epithelial sheet migration. New J Phys 15(2):025036

36. Liang CC, Park AY, Guan JL (2007) In vitro scratch assay: a convenient and inexpensive method for analysis of cell migration in vitro. Nat Protoc 2(2):329–333. doi:10.1038/nprot.2007.30

37. Kolega J (2006) The role of myosin II motor activity in distributing myosin asymmetrically and coupling protrusive activity to cell translocation. Mol Biol Cell 17(10):4435–4445

38. Mironmendoza M, Graham E, Kivanany PB, Quiring J, Petroll WM (2015) The role of thrombin and cell contractility in regulating clustering and collective migration of corneal fibroblasts in different ECM environments. Invest Ophthalmol Vis Sci 56(3):2079–2090

39. Ng MR, Besser A, Danuser G, Brugge JS (2012) Substrate stiffness regulates cadherin-dependent collective migration through myosin-II contractility. J Cell Biol 199(3):545–563. doi:10.1083/jcb.201207148

40. Raffel M, Willert CE, Kompenhans J (2013) Particle image velocimetry: a practical guide. Springer, New York

41. Vitorino P, Meyer T (2008) Modular control of endothelial sheet migration. Genes Dev 22(23):3268–3281

42. Nnetu KD, Knorr M, Kas JA, Zink M (2012) The impact of jamming on boundaries of collectively moving weak-interacting cells. New J Phys 14(11):115012

43. Sepulveda N, Petitjean L, Cochet O, Graslandmongrain E, Silberzan P, Hakim V (2013) Collective cell motion in an epithelial sheet can be quantitatively described by a stochastic interacting particle model. PLoS Comput Biol 9(3):e1002944

44. Masuzzo P, Van Troys M, Ampe C, Martens L (2016) Taking aim at moving targets in computational cell migration. Trends Cell Biol 26(2):88–110

45. Vitorino P, Hammer MM, Kim J, Meyer T (2011) A steering model of endothelial sheet migration recapitulates monolayer integrity and directed collective migration. Mol Cell Biol 31(2):342–350

46. Szabo B, Szollosi GJ, Gonci B, Juranyi Z, Selmeczi D, Vicsek T (2006) Phase transition in the collective migration of tissue cells: experiment and model. Phys Rev E 74(6):061908

47. Kusch J, Liakopoulos D, Barral Y (2003) Spindle asymmetry: a compass for the cell. Trends Cell Biol 13(11):562–569. doi:10.1016/j.tcb.2003.09.008

48. Vladar EK, Antic D, Axelrod JD (2009) Planar cell polarity signaling: the developing cell's compass. Cold Spring Harbor Perspect Biol. doi:10.1101/cshperspect.a002964

49. Rickert P, Weiner OD, Wang F, Bourne HR, Servant G (2000) Leukocytes navigate by compass: roles of PI3Kγ and its lipid products. Trends Cell Biol 10(11):466–473. doi:10.1016/S0962-8924(00)01841-9

50. Arrieumerlou C, Meyer T (2005) A local coupling model and compass parameter for eukaryotic chemotaxis. Dev Cell 8(2):215–227. doi:10.1016/j.devcel.2004.12.007

51. Tsai F-C, Seki A, Yang H, Hayer A, Carrasco S, Malmersjö S, Meyer T (2014) A polarized Ca^{2+}, diacylglycerol and STIM1 signalling system regulates directed cell migration. Nat Cell Biol 16(2):133–144. doi:10.1038/ncb2906

52. Brundage RA, Fogarty KE, Tuft RA, Fay FS (1991) Calcium gradients underlying polarization and chemotaxis of eosinophils. Science 254(5032):703–706

53. Lee J, Ishihara A, Oxford G, Johnson B, Jacobson K (1999) Regulation of cell movement is mediated by stretch-activated calcium channels. Nature 400(6742):382–386

54. Hahn K, DeBiasio R, Taylor DL (1992) Patterns of elevated free calcium and calmodulin activation in living cells. Nature 359(6397):736–738

55. Janmey PA (1994) Phosphoinositides and calcium as regulators of cellular actin assembly and disassembly. Annu Rev Physiol 56(1):169–191

56. Mandeville J, Ghosh RN, Maxfield FR (1995) Intracellular calcium levels correlate with speed and persistent forward motion in migrating neutrophils. Biophys J 68(4):1207

57. Tran POT, Hinman LE, Unger GM, Sammak PJ (1999) A wound-induced $[Ca^{2+}]_i$ increase and its transcriptional activation of immediate early genes is important in the regulation of motility. Exp Cell Res 246(2):319–326

58. Kohn EC, Alessandro R, Spoonster J, Wersto RP, Liotta LA (1995) Angiogenesis: role of calcium-mediated signal transduction. Proc Natl Acad Sci 92(5):1307–1311

Cellular and Molecular Life Sciences

Supplementary Materials

Collective Cell Migration has Distinct Directionality and Speed Dynamics

Yan Zhang[1,2,3], Guoqing Xu[4,5], Rachel M Lee[6], Zijie Zhu[3], Jiandong Wu[4], Simon Liao[5], Gong Zhang[7,8], Yaohui Sun[1], Alex Mogilner[9], Wolfgang Losert[6], Tingrui Pan[3], Francis Lin[4,*], Zhengping Xu[2,*], Min Zhao[1,10*]

[1] Department of Dermatology, University of California, Davis, CA 95616, USA.

[2] Institute of Environmental Medicine, Zhejiang University School of Medicine, 866 Yuhangtang Rd., Hangzhou 310058, China.

[3] Micro-Nano Innovations (MiNI) Laboratory, Department of Biomedical Engineering, University of California, Davis, CA 95616, USA.

[4] Department of Physics and Astronomy, University of Manitoba, Winnipeg, MB, R3T 2N2, Canada.

[5] Department of Applied Computer Science, University of Winnipeg, Winnipeg, MB, R3B 2E9, Canada.

[6] Department of Physics, University of Maryland, College Park, MD 20742, USA.

[7] Seven Oaks Hospital Wellness Institute, 1075 Leila Ave, Winnipeg, MB R2P 2W7, Canada.

[8] The First Affiliated Hospital of Henan University of Science and Technology, 24 Jinghua Rd., Luoyang, 471003, China.

[9] Courant Institute and Department of Biology, New York University, 251 Mercer Street, New York, NY 10012, USA.

[10] Department of Ophthalmology and Vision Science, University of California, Davis, CA 95616, USA.

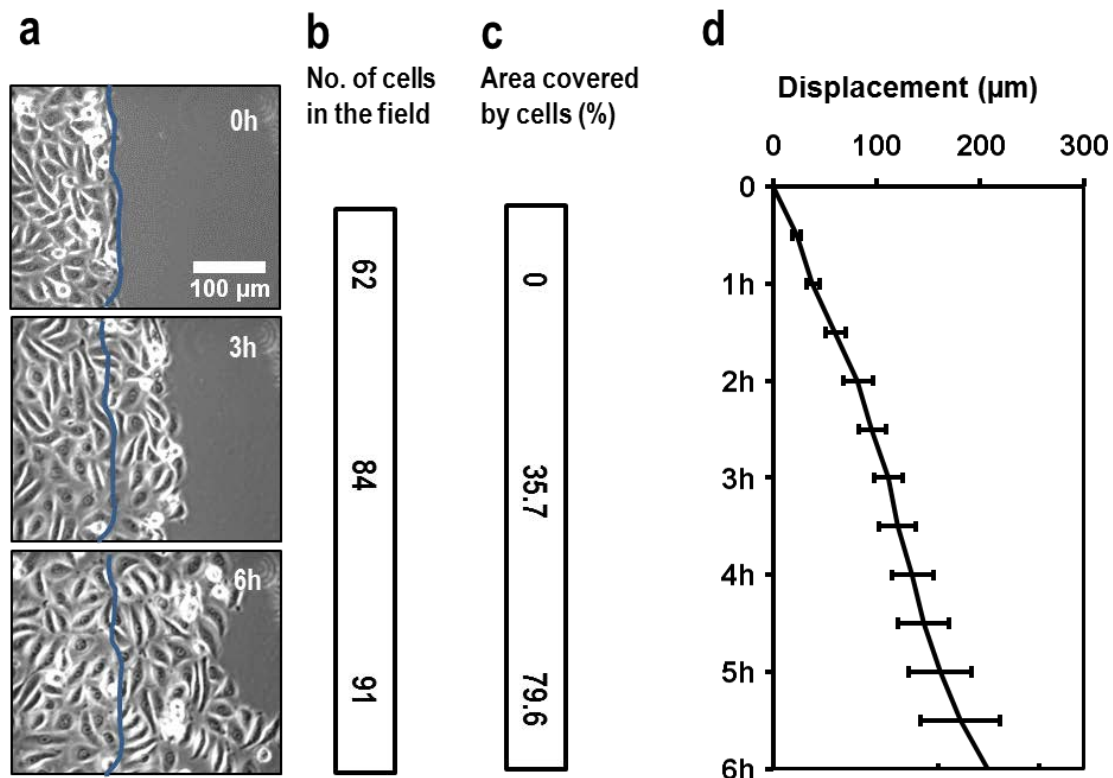**Correspondence:** minzhao@ucdavis.edu, zpxu@zju.edu.cn Or flin@physics.umanitoba.ca.

a Time-lapse images showing the directional migration of epithelial cells after removal of the PDMS barrier on the right. **b** The number of cells in the field at each time point. **c** Percentage of the originally cell-free area covered by migrating cells. **d** Migration of the leading edge into the cell-free area. The distance that the leading edge advanced in the horizontal axis was plotted against time. Human corneal epithelial (HCE) cells were cultured to confluence against a PDMS strip. Time lapse video was recorded after removing the strip. Bar = 100 µm; time as shown. Values are mean ± S.E.M. from 3 independent experiments.
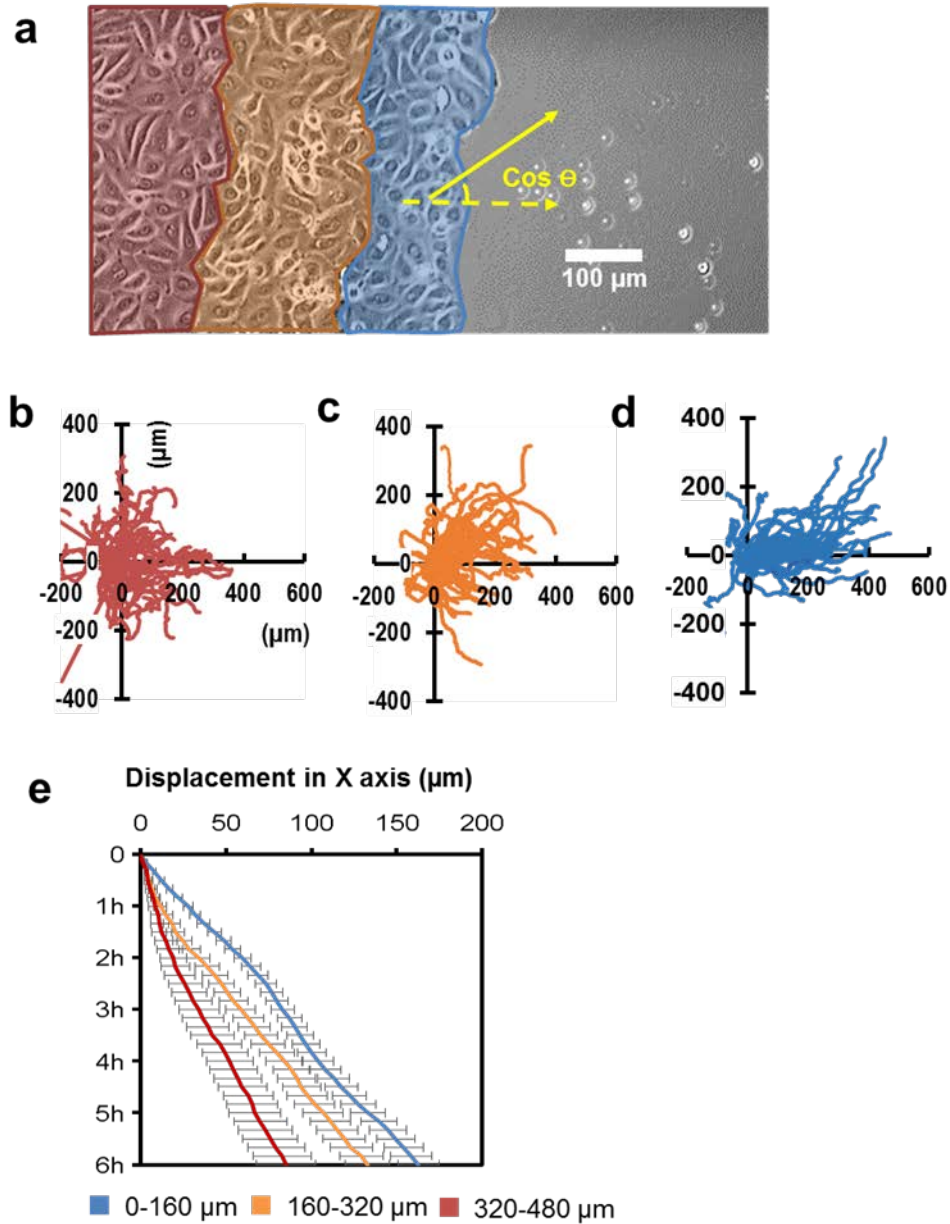
Fig. S2 Regional difference in cell migration following removal of the PDMS barrier.

a Cells were divided into three regions of ~5 cell rows from the free edge: 0-160 µm (Blue), 160-320 µm (Orange), 320-480 µm (Red). **b**, **c**, **d** Cells in the three regions showed different directional migration responses. All cell positions at time zero are normalized to the origin of the graph (0, 0). **e** Time-dependent migration of cells in the three regions along the x-axis; cells migrating to wound edge have positive displacement. Bar = 100 µm; time as shown. Values are mean ± S.E.M. from 3 independent experiments.
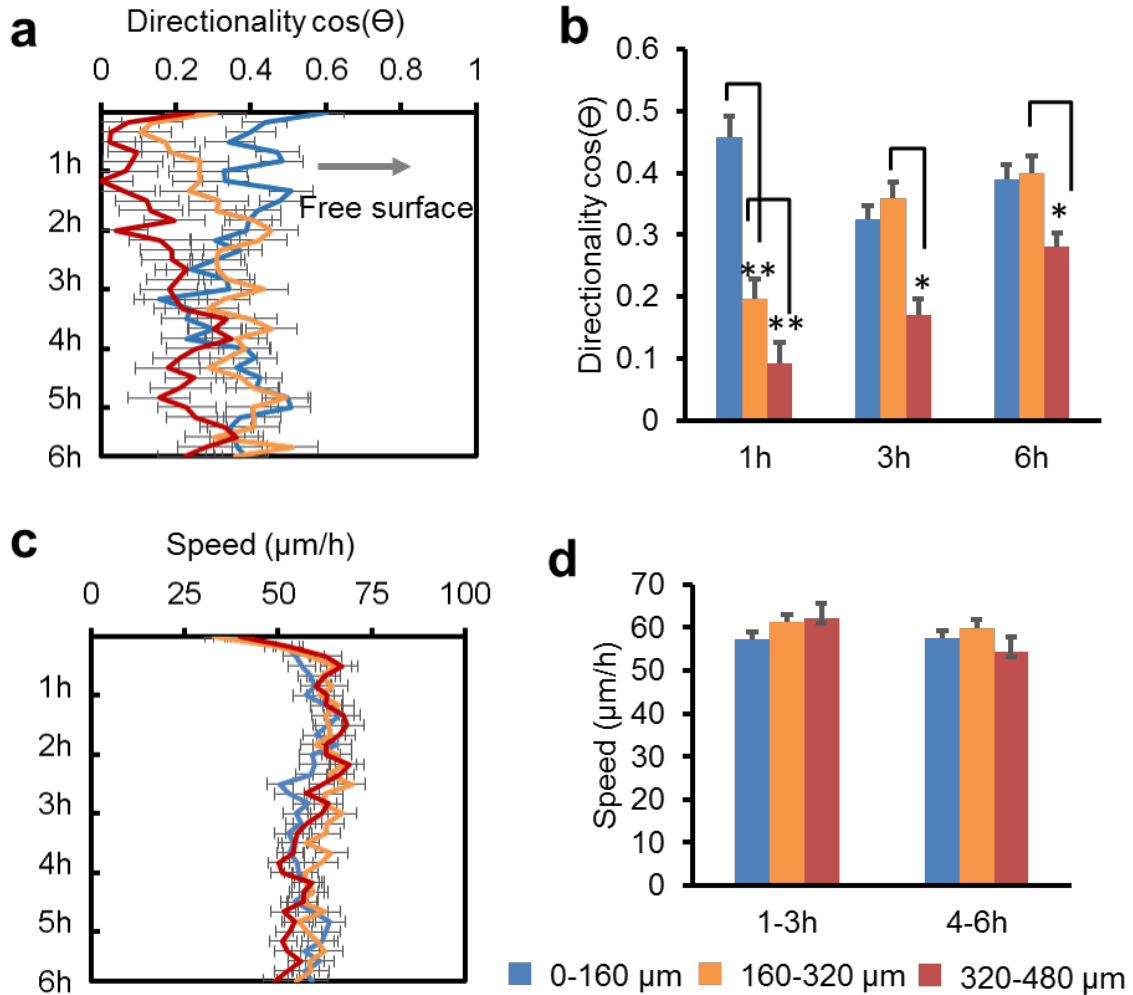
Fig. S3 Free edge induced region-dependent changes in directionality, but not in the speed of cell migration.

a Cell migration directionality in the three regions. In all graphs, blue = close to edge, orange = middle region, red = far from edge. **b** Directionality (cos Θ) of cells in the three distinct regions at 1 h, 3 h and 6 h. **c** Cell migration speed (µm/h) in the three regions. **d** Cell migration speed in the three distinct regions at 1 h, 3 h and 6 h. Directionality and speed here are calculated by manual individual cell tracking. n = 75~108 cells. *$p < 0.05$, and **$p < 0.01$. Shown is mean ± S.E.M. from 4 independent experiments.
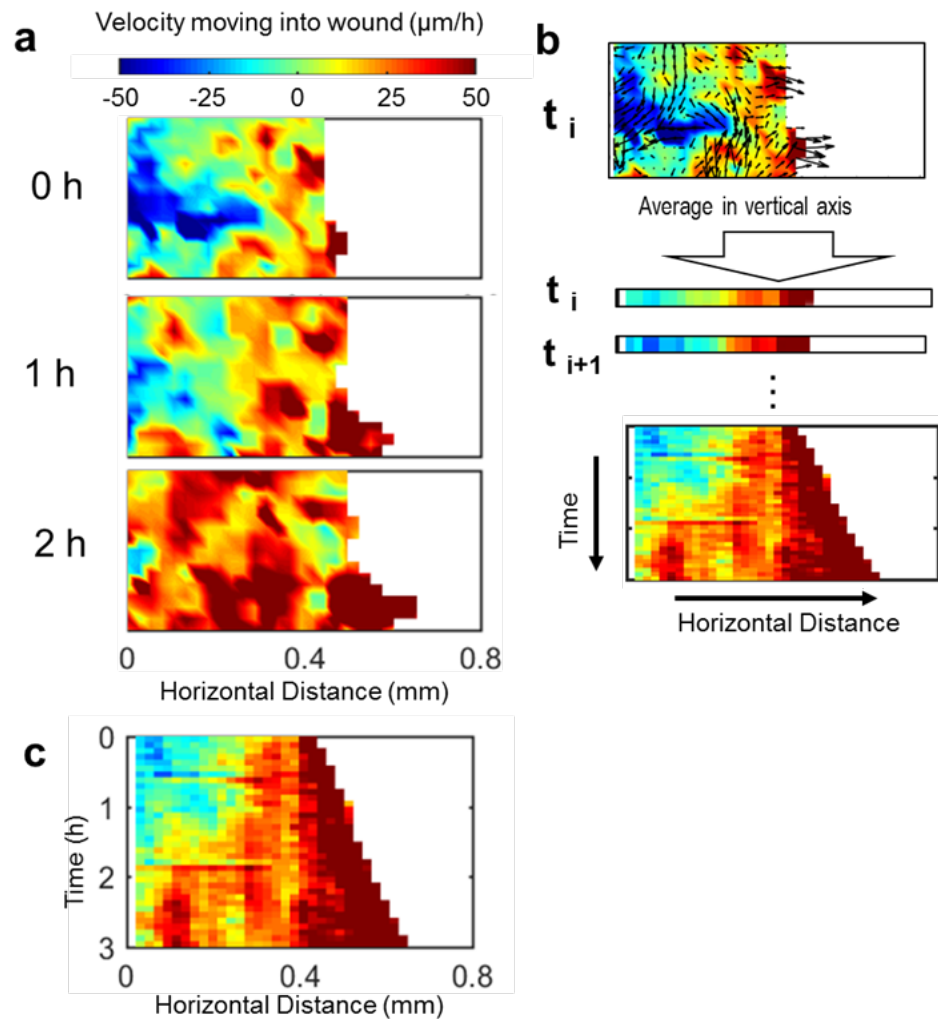
Fig. S4 Cells migrated directionally into cell-free areas following PDMS barrier removal, velocity moving into wound increased (accelerated) which propagated into the cell sheet like a wave.

a Heat maps are snapshots of velocity moving into the wound (horizontal velocity/X-axis velocity) revealed by the PIV analysis of a cell sheet at 0 h, 1 h, and 2 h. **b** Computing spatiotemporal maps (kymographs). For each heat map, the mean value (ignoring acellular area) of each column was plotted on a strip according to the color map. Horizontal velocity directed to the cell-free area would have a positive value. Horizontal velocity to the left would be negative. The kymograph is generated by laying out the strips following the time. **c** Kymographs for speed moving into wound shows the increase of speed moving into the wound at the leading edge and the increase in horizontal velocity in the cell sheet propagated into the sheet as a wave moving backward (also see *A* above). Color shows the value of horizontal velocity from -50 µm/h to 50 µm/h. High speed horizontally towards the right (to the cellular area) is shown with colors biased to the red, whereas higher speed horizontally towards left (away from the free edge) shows in color biased to the blue. Snapshots and kymograph were from one typical experiment.
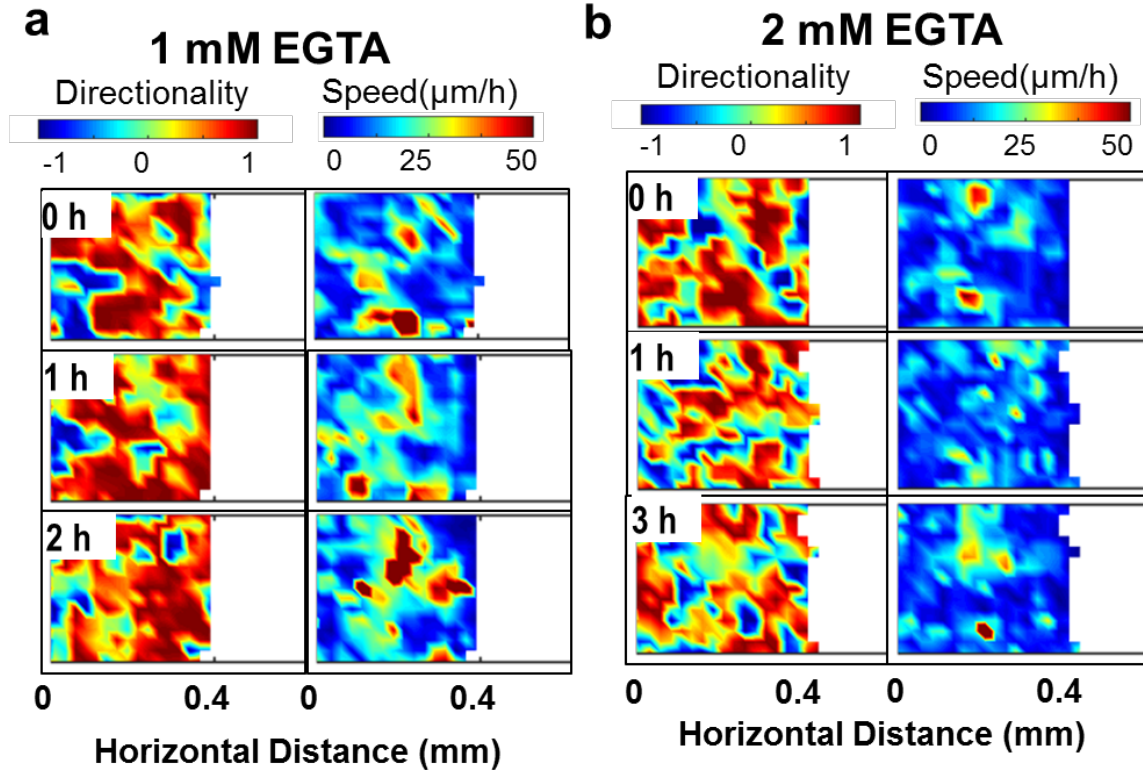
Fig. S5 EGTA treatment abolished directionality wave propagation.

Snapshots of heat maps of directionality and speed from PIV analysis after 1 mM EGTA treatment at **a**, or 2 mM EGTA treatment at **b**. The directionality of cell migration was quantified using cosine theta (see Materials and Methods for details). Color shows the value of cosine theta from -1 to 1. Regions which migrated directionally towards the right (to the acellular area) show colors biased to the red, whereas cells which migrated to the left show color biased to the blue. Color codes for speed range from 0 to 50 µm/h without any indication of directionality.
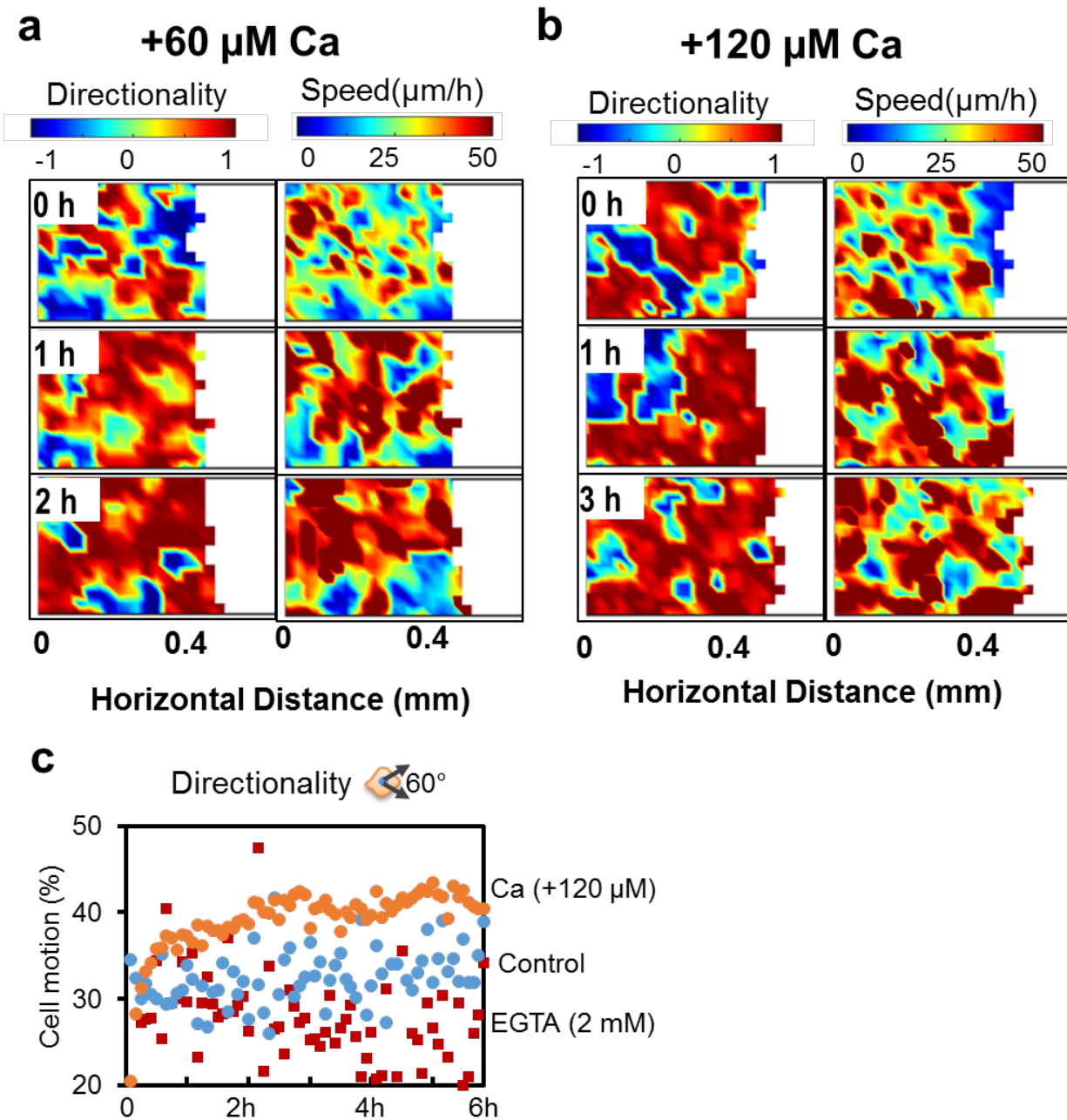
Fig. S6 Additional Calcium treatments promote directionality wave propagation.

Snapshots of heat maps of directionality and speed from PIV analysis after additional calcium treatment at 60 µM **a**, or 120 µM **b**. The directionality of cell migration was quantified using cosine theta (see Materials and Methods for details). Color shows the value of cosine theta from -1 to 1. Cells migrated more directionally towards the right (to the acellular area) showed colors biased to the red, whereas cells migrated to the left showed color biased to the blue. Color codes the speed range without any indication of directionality. **c** High Ca^{2+} significantly increased collective directionality. The graph shows the time course of the proportion of cells motion directed to the free edge within a bias angle less than 60 degrees in control (blue), EGTA treated (2 mM; red), high calcium (+120 µM; orange) groups.

7
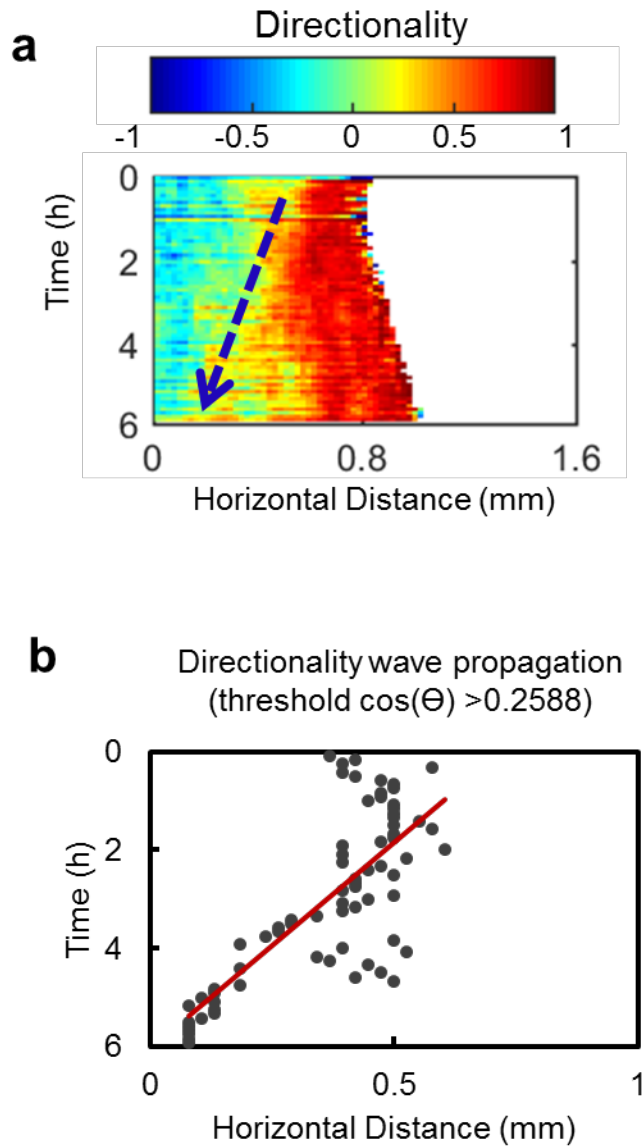
Fig. S7 Quantification of the rate of directionality wave propagation.

a Characteristic directionality wave in a kymograph of directionality. **b** The plot of the front of the directionality waves against time. The points stand for the front of the directionality wave against each time interval. The red line is the linear fit of the points. The slope of the linear fit is *a*. The propagation rate of the directionality wave is defined as R = 1/a. (Please see the Materials and Methods for details)

Fig. S8 Blebbistatin treatment did not affect overall cell migration and directionality wave propagation.

a The field were divided into six regions, three regions (NO. 1, 2, 3) on the right of the free edge and three regions (NO. 4, 5, 6) on the left of the free edge at the beginning of imaging, each region was 160 µm in w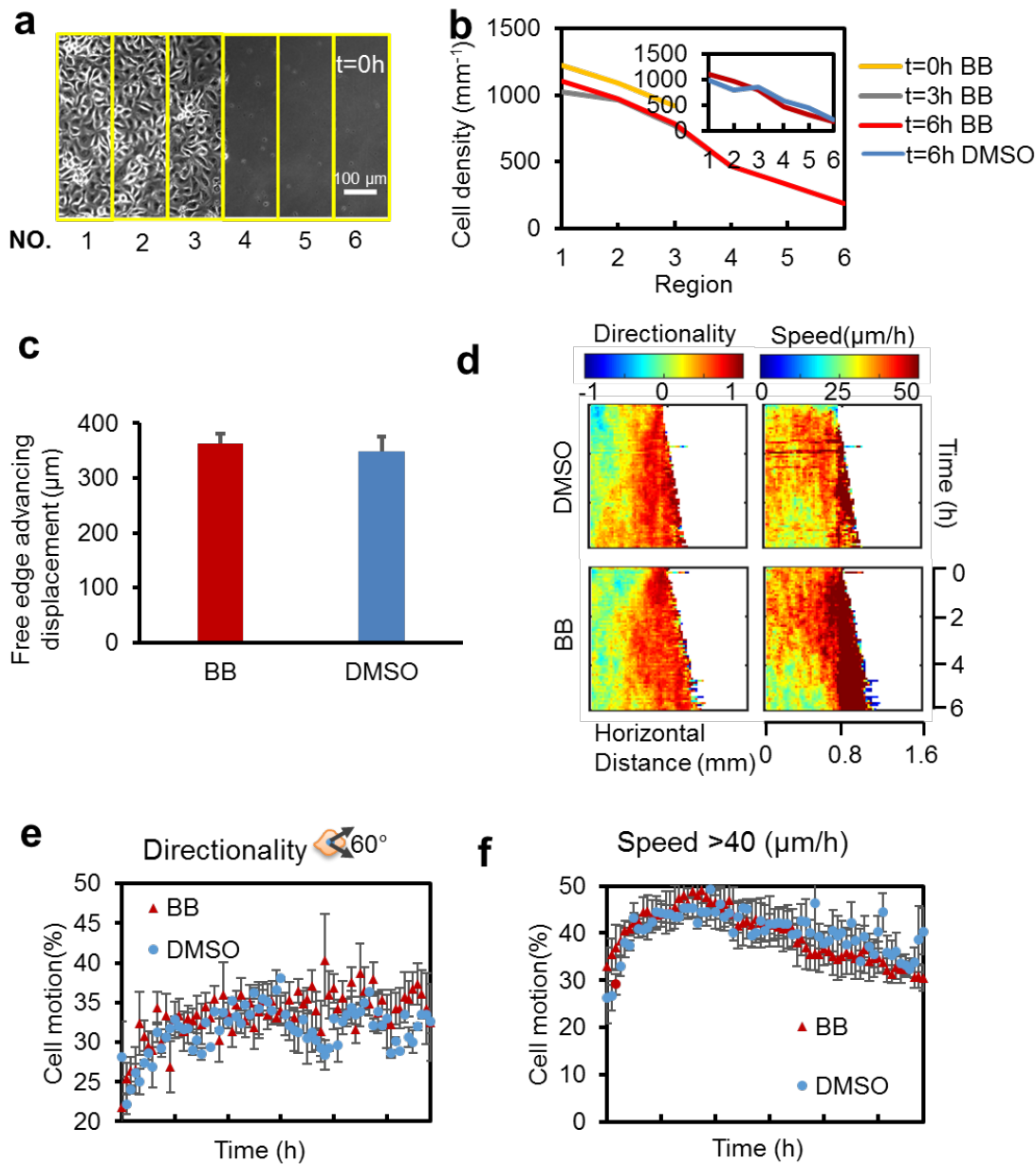idth. Bar = 100 µm. **b** Cell density on different regions at 1 h, 3 h and 6 h for blebbistatin-treated group and DMSO control group. **c** Advancement of the leading edge into the cell-free area for 6 h after peeling PDMS barrier. No significance difference was found between blebbistatin-treated group and DMSO control group. **d** Kymographs suggest that blebbistatin had no significant effects on directionality wave propagation and speed. Color indicates the value of cosine theta (directionality) from -1 to 1 or the cell speed from zero to 50 µm/h. **e-f** After PDMS barrier removal, no significant difference in the proportion of cell motion directed to the free edge within a bias angle less than 60 degrees and the fraction of cells with a speed over 40 µm/h were found. Directionality and speed of cell migration

9

were calculated using PIV (see Materials µand Methods). Data are presented as mean ± S.E.M. from three independent experiments.

Supplementary Movie legends

Video S1. A time-lapse phase contrast video of directional cell collective migration after peeling off a PDMS barrier. The timestamp is in minutes. Bar = 100 µm.

Video S2. A time-lapse video of directionality and speed derived from PIV. Color codes the cell migration directionality and speed. The timestamp is in minutes. The still images shown in Fig. 1a, b are derived from Video S2.

Video S3. Simulation of the control group in the Particle-Based Compass model. Each ball (blue) indicates one cell. The arrow (orange) indicates the directionality.

Video S4. Time-lapse phase contrast videos of directional cell collective migration after peeling off PDMS barrier for calcium intervention groups. The timestamp is in minutes. Bar = 100 µm.

Video S5. A time-lapse video of directionality and speed derived from PIV for 1 mM EGTA group. Color codes the directionality and speed. The timestamp is in minutes. The still images shown in Supplementary Fig. S5a are derived from Video S4.

Video S6. A time-lapse video of directionality and speed derived from PIV for the 120 µM Calcium group. Color codes the cell migration directionality and speed. The timestamp is in minutes. The still images shown in Supplementary Fig. S6b are derived from Video S6.

Video S7. Time-lapse phase contrast videos of directional cell collective migration after peeling off PDMS barrier for blebbistatin-treated group and control group. The timestamp is in minutes. Bar = 100 µm

Supplementary Experimental Procedures

PIV analysis

Cell migration was measured by calculating intensity correlations between subsequent images of the time-lapse imaging using MATLAB (MathWorks) with a custom-made MATLAB code based on MatPIV1.6.1 (freeware distributed under the terms of the GNU general public license). In brief, the program split each frame into first 64x64 pixel^2 and then 32x32 pixel^2 interrogation windows with 50% overlap. The time interval between consecutively analyzed images was 5 min. The respective displacement vector for each interrogation window between subsequent frames was calculated. A mask based on the gradient of the image was applied to eliminate the cell-free region for each frame and remove the background. Boundary effects of PIV were suppressed by eroding 8 pixels from the edge of the cell sheet. To eliminate velocity components caused by unspecific movements of microscope, these time-lapse stacks were registered ('Register Virtual Stack' command; Image J) before PIV analysis. The PIV output thus provides u (horizontal velocity) and v (vertical velocity) for 16x16 pixel^2 regions within the cell sheet on the time scale of 5 min. Speed was calculated using Speed $= \sqrt{u^2 + v^2}$. Directionality was defined as the cosine of the angle between the velocity vector and u ($\cos\theta = u / \sqrt{u^2 + v^2}$). A flow vector towards the free surface would have a cosine value of 1. A flow vector parallel to the free edge would have a cosine value of 0, while a vector towards away from the wound edge would have a cosine value of -1.

Particle-Based Compass model for collective cell migration

We developed a Particle-Based Compass (PBC) model to study directionality wave propagation during collective cell migration in a 2D wound healing assay. This model successfully captured the key experimental observations, particularly the characteristics of directionality wave propagation.

In this model, all cells are treated as physical particles with identical size. The area centered at a specific cell is divided into eight equal sectors (Fig. 2). The angle range for the nth angular sector is $[-\pi/8 + (\pi/4)*n, \ \pi/8 + (\pi/4)*n]$, where $n = [1, 2, ... 8]$.

We assume that if the distance d between the kth cell and its nearest neighboring cell in a particular angular sector is less than the repulsive threshold distance D_0, the kth cell will have a repulsive interaction with the neighbor cell. The magnitude of this repulsive interaction is inversely proportional to d. If d is greater than the free edge threshold distance D_{max} in one angular sector, a constant vector will be assigned to this cell for this angular sector, with the angle of this vector points towards the middle of the angular sector. If d is between D_0 and D_{max}, the kth cell experiences an attractive interaction toward the nearest neighboring cell. The magnitude of this biased directionality is directly proportional to d. Thus, the cell-cell interaction for the kth cell in the nth angular quadrant at time t is summarized as the following:

$$\vec{p}_{kn}(t) = \begin{cases} -\dfrac{D_0}{\left|\vec{p}_{knm}(t)\right|} * \widehat{p}_{knm}(t), \text{if } (0 < \left|\vec{p}_{knm}(t)\right| \leq D_0) \\[2em] \dfrac{\left|\vec{p}_{knm}(t)\right|}{D_0} * \widehat{p}_{knm}(t), \text{if } (D_0 < \left|\vec{p}_{knm}(t)\right| \leq D_{max}) \\[2em] \dfrac{D_{max}}{D_0} * \widehat{p}_{def}, \text{ if } (\left|\vec{p}_{knm}(t)\right| > D_{max}) \end{cases} \qquad (1)$$

Where $\widehat{p}_{knm}$ is the unit vector pointing from the kth cell toward its nearest neighboring cell in the nth sector, the subscript m denotes the minimal distance from the kth cell to the nearest neighboring cell in the nth sector and $\widehat{p}_{def}$ is the unit vector pointing toward the middle angle of the nth sector.

$$\text{Thus, } d = \left| \vec{p}_{knm}(t) \right|. \qquad (2)$$

This mechanism is applied to compute the cellular interplay vector in each of the eight angular sectors. By summing up the eight cellular interplay vectors, the total cellular interplay vector for a specific cell can be obtained.

$$\vec{p}_k(t) = \sum_{n=1}^{8} \vec{p}_{kn}(t) \qquad (3)$$

The phase of this vector will be used to determine the cell migration angle for the kth cell at time t.

$$\theta_k(t) = \angle \vec{P}_k(t) \qquad (4)$$

The migration angle and the constant cell speed are used to compute the displacement of the kth cell over each time step and thus to update the cell's coordinates, using the equation

$$x_k(t+1) = x_k(t) + S * \cos\theta_k(t) \qquad (5)$$

$$y_k(t+1) = y_k(t) + S * \sin\theta_k(t) \qquad (6)$$

where S is the cell migration speed.

This algorithm is used to simulate collective cell migration as in the experimental wound healing assay. In the computer simulation, the cell array is configured as a rectangular shape. All the length parameters were scaled such that 0.1 in model length units equals 20 µm in real space (equivalent to the diameter of a single cell). The speed for the control group is set as 0.015 model length units (3 µm in real space) per time step (4.8 min in real time) with normalized distributed noise (standard deviation = 0.001) in the simulation, which is equivalent to the average speed of 37.3 µm/h in the experimental control group. The value of D_{max} should be larger than the cell-cell distance of two completely expanded cells (>0.2), so we set it at 0.30 (60 µm in real space). Cells are packed and compressed at the beginning of the experiment (Supplementary Video S1) and there should to be a repulsive effect between cells at $d = 0.1$, so the repulsive threshold distance should be larger than 0.1. After a systematic test, D_0 in the control group simulation is set at 0.12 (24 µm in real space) to best match the propagation rate of directionality wave observed in cell experiment. The cell speed in the EGTA group simulation was reduced to 30% of the control group (i.e. 30%×37.3 µm/h = 11.2 µm/h).

Detailed parameter descriptions for the model are shown in Table S1.

Table S1. Parameters in the PBC model

Symbols	Implications	Values (unit)
N	Total number of simulated cells	3500
x_k	x coordinate of the kth cell	Variable
y_k	y coordinate of the kth cell	Variable
θ_k	Migration angle of kth cell	Variable (radian)
n	Denoting the nth angular sector with the angle range: $[-\pi/8 + (\pi/4)*n, \ \pi/8 + (\pi/4)*n]$	Integers 1-8
$\vec{p}_k$	Cellular interplay vector for the kth cell	Variable

$\vec{p}_{kn}$	Cellular interplay vector for the kth cell in the nth sector	Variable
$\vec{p}_{knm}$	Vector from the kth cell to the nearest neighboring cell in the nth sector	Variable
$\widehat{p}_{def}$	Unit vector towards the middle angle of the kth sector	Variable
$\widehat{p}_{knm}$	Unit vector from the kth cell to the nearest neighboring cell in the nth sector	Variable
S	Cell migration speed	Variable
		Control group: $S = 0.015$
D_0	Repulsive threshold (cell-cell distance)	Variable
		Control group: $D_0 = 0.12$
D_{max}	Free edge motion threshold (cell-cell distance)	Variable
		Control group: $D_{max} = 0.30$

We have presented a two-dimensional physical model based on experimental data. This model recreates characteristics similar to wound healing assay experiments, especially directionality wave propagation patterns and the influence of cell velocities on directionality waves. The entire process could be reproduced in minutes by running our program. By computing the distances between cells and assigning different weights to their moving angles, we show how the dynamics of individual cell motion could affect the coordinated migration of its neighboring cells.

The key concept of collective cell migration is coordinated motion of a group of cells by cell-cell interactions. The underlying mechanism of cell-cell interactions in collective cell migration is complex and far from being clearly understood. Our current PBC model approaches the cell-cell interactions by applying a repulsive or attractive force among neighboring cells depending on the cell-cell distance. The simulation results successfully captured some of the dynamic features of the wound healing experiments, suggesting the effectiveness of this simple PBC model. Physical force based models for collective cell migration can be associated with some well-known biophysical mechanisms such as contact inhibition of locomotion and free-space signal [1], compressive deformation of cell morphology, elasticity of cytoskeleton and plasma membrane, and intercellular adhesions [2]. Although these physical models do not directly investigate the underlying biochemical mechanisms for regulating cell-cell interaction, they are useful for understanding the system-level properties of multi-cellular migratory behaviors. In our PBC model, one key parameter is the threshold cell-cell distance D_0 for switching from repulsive to attractive cell-cell interaction. Without knowing the exact strength of cell-cell interactions, we inversely mapped the magnitude of repulsive cell-cell interaction to the cell-cell distance up to D_0 and linearly mapped the attractive cell-cell interaction to the cell-cell distance beyond D_0. This simplistic mapping strategy is conceptually similar to the cell-cell distance based interaction function derived from other relevant models [3]. In our model, the attractive/repulsive interaction values are not continuous over cell-cell distance. It would be more realistic if the interaction is modeled as a continuous function of d, but it will not affect the general results. Interestingly, in a non-particle based computer model of cell group migration, Coburn *et al.* found that, with contact inhibition of locomotion only, single cells under constraint moved coherently after a considerable period of time [4]. For cells

without firm connection, contact inhibition of locomotion alone may be enough to trigger directional collective migration. On the other hand, it is worth clarifying that the attractive cell-cell interaction in our PBC model reflects not only physical cell connection between neighboring cells but also a free-space signal to induce cell migration toward the less crowded space (i.e. the wound) as the border cells.

We find that after reducing cell velocity to 30% in the simulations (a value similar to those seen in EGTA experiments), the directionality wave could still propagate from border cells to inner cells, but with a lower propagation rate compared to the control simulation. This is consistent with experiment data. We also find some physical parameters, like the repulsive threshold D_0 and free edge threshold D_{max}, which could have significant influences on collective cell migration. The repulsive parameter D_0 is a very significant parameter; by reducing D_0, we find directionality waves propagate faster. By increasing the cell velocity S, the directionality wave also propagates faster. Thus, the modeling would allow us to explore different experimental conditions through simple modifications of these parameters.

Our model assumed a constant speed for all cells and thus did not capture the experimental velocity pattern. In reality, different cells have different velocities. Even for a single cell, its velocity can vary over time. It is also worth pointing out that our PBC model is designed for collective cell migration. For simplicity, we did not include noise for the cell's final orientation. Therefore, the single cell migration mode is neglected in our model. Future modeling work will consider the synergetic effect of directionality and velocity of collective cell migration and will include single cell migration mode and more realistically model the cell-cell interaction forces.

Supplementary Reference

1. Camley BA, Zimmermann J, Levine H, Rappel W-J (2016) Emergent collective chemotaxis without single-cell gradient sensing. Physical review letters 116 (9):098101
2. Yamao M, Naoki H, Ishii S (2011) Multi-cellular logistics of collective cell migration. PloS one 6 (12):e27950
3. Gruler H, de Boisfleury-Chevance A (1994) Directed cell movement and cluster formation: physical principles. Journal de Physique I 4 (7):1085-1105
4. Coburn L, Cerone L, Torney CJ, Couzin ID, Neufeld Z (2013) Tactile interactions lead to coherent motion and enhanced chemotaxis of migrating cells. Physical Biology 10 (4):046002